SUPPLEMENTARY TEXT S1

Exploring the role of GS-GOGAT cycle in microcystin synthesis and regulation – a model based analysis

SWARNENDU BANERJEE, ABHISHEK SUBRAMANIAN, JOYDEV CHATTOPADHYAY, RAM RUP SARKAR

S1. Reactions considered in the model

The following reactions have been considered in the model:

Table S1: Reactions considered in the model

Reactions	Reference
$glutamine + 2\text{-}OG \xrightarrow[GOGAT]{v_{max1}} glutamate$	17
$glutamate + NH_4^+ \xrightarrow[GS]{v_{max2}} glutamine$	17
$NH_4^+ + 2\text{-}OG \xrightarrow[GDH]{v_{max3}} glutamate$	17
$NtcA + 2\text{-}OG \underset{b_{aa}}{\overset{f_{aa}}{\rightleftarrows}} NtcA^{(a)}$	21
$NtcA^{(a)} + PipX \underset{b_{ax}}{\overset{f_{ax}}{\rightleftarrows}} NtcA^{(a)}\text{-}PipX$	23
$PII + PipX \xrightarrow{f_{px}} PII\text{-}PipX$	23
$PII\text{-}PipX \xrightarrow[2-OG]{b_{px}} PII + PipX$	23, 25
$glutamate \xrightarrow[Mcy]{f_{mg}} Microcystin$	6, 18

S2. Positive invariance

Let, $X = ([NH^{+}_{4(ext)}],[Glu],[Gln],[2\text{-}OG],[NH^{+}_{4}],[NtcA],[NtcA^{(a)}],[PII],[PipX],$ $[NtcA^{(a)}\text{-}PipX],[PII\text{-}PipX],[Mcy],[MC])^{T} \in \mathbb{R}^{13}$ and $F(X) = [F_1(X), F_2(X), F_3(X), F_4(X), F_5(X), F_6(X), F_7(X), F_8(X), F_9(X), F_{10}(X), F_{11}(X), F_{12}(X), F_{13}(X)]$ with $F : C_+ \to \mathbb{R}^{13}$ and $F \in C^{\infty}(\mathbb{R}^{13})$. Then the system of differential equations (7) becomes $\dot{X} = F(X)$ where $X(0) = X_0 \in \mathbb{R}^{13}_{+}$. It is easy to check that $F_i(X) \mid X_i = 0 \geq 0$ and hence any solution of the above system with $X_0 \in \mathbb{R}^{13}_{+}$, say, is such that $X(t) \in \mathbb{R}^{13}_{+}$ for all t > 0.

S3. Boundedness

Theorem: All solutions of the system of differential equation (7) are uniformly bounded.

Let, $W_1 = [NH^{+}_{4(ext)}] + [Glu] + [Gln] + [2\text{-}OG] + [NH^{+}_{4}] + [NtcA^{(a)}] + [PII] + [NtcA^{(a)}\text{-}PipX] + [PII\text{-}PipX] + [Mcy] + [MC]$

Then taking time derivative and using the equation, we have,

$$\frac{dW_1}{dt} \leq l_{w1} - V_{GS} - V_{GOGAT} - V_{GDH} + k_m\left(\frac{[NtcA^{(a)}]^3}{\theta_3 + [NtcA^{(a)}]^3} + \frac{[NtcA^{(a)}\text{-}PipX]^3}{\theta_4 + [NtcA^{(a)}\text{-}PipX]^3}\right) - d_{w1}W_1$$

where, $d_{w1} = min\left\{d_N, d_{gl}, d_{gn}, d_{og}, d_n, d_{aa}, d_p, d_{ax}, d_{px}, d_m, d\right\}$

and $l_{w1} = L + l_{nh} + l_{gl} + l_{gn} + l_{og} + l_p + l_{mcy}$

$$\Rightarrow \frac{dW_1}{dt} \leq (l_{w1} + 2k_m) - d_{w1}W_1 \text{ since } k_m\left(\frac{[NtcA^{(a)}]^3}{\theta_3 + [NtcA^{(a)}]^3}\right) \leq k_m \text{ and so on.}$$

$$\Rightarrow \frac{dW_1}{dt} + d_{w1}W_1 \leq \Omega_1 \text{ where, } \Omega_1 = l_{w1} + 2k_m$$

From the theory of differential inequalities,[38] we then obtain,

$$0 < W_1([NH^{+}_{4(ext)}],[Glu],[Gln],[2\text{-}OG],[NH^{+}_{4}],[NtcA^{(a)}],[PII],[NtcA^{(a)}\text{-}PipX],[PII\text{-}PipX],[Mcy],[MC])$$

$$< \frac{\Omega_1}{d_{w1}}(1-e^{-d_{w1}t}) + W_1([NH^+_{4(ext)}](0),[Glu](0),[Gln](0),[2\text{-}OG](0),[NH^+_4](0),[NtcA^{(a)}](0),$$

$$[PII](0),[NtcA^{(a)}\text{-}PipX](0),[PII\text{-}PipX](0),[Mcy](0),[MC](0))e^{-d_{w1}t}$$

and for $t \to \infty$, it follows $0 < W_1 < \frac{\Omega_1}{d_{w1}}$, hence all solutions of

$$([NH^+_{4(ext)}](t),[Glu](t),[Gln](t),[2\text{-}OG](t),[NH^+_4](t),[NtcA^{(a)}](t),[PII](t),[NtcA^{(a)}\text{-}PipX](t),$$

$[PII\text{-}PipX](t),[Mcy](t),[MC](t))$ that initiate at

$$([NH^+_{4(ext)}](0),[Glu](0),[Gln](0),[2\text{-}OG](0),[NH^+_4](0),[NtcA^{(a)}](0),[PII](0),[NtcA^{(a)}\text{-}PipX](0),$$

$[PII\text{-}PipX](0),[Mcy](0),[MC](0))^T \in \mathbb{R}^{11}$ are confined to the region :

$$G_1 = \{([NH^+_{4(ext)}],[Glu],[Gln],[2\text{-}OG],[NH^+_4],[NtcA^{(a)}],[PII],[NtcA^{(a)}\text{-}PipX],[PII\text{-}PipX],$$

$[Mcy],[MC])^T \in \mathbb{R}^{11} : W_1 = \frac{\Omega_1}{d_{w1}} + \epsilon_1$ for any $\epsilon_1 > 0\}$ for all $t \geq T^*$, where T^* depends on initial values $([NH^+_{4(ext)}](0),[Glu](0),[Gln](0),[2\text{-}OG](0),[NH^+_4](0),[NtcA^{(a)}](0),[PII](0),$

$[NtcA^{(a)}\text{-}PipX](0),[PII\text{-}PipX](0),[Mcy](0),[MC](0))^T$.

Again let, $W_2 = [NtcA] + [PipX]$

Then we have,

$\frac{d[NtcA]}{dt} \leq l_a + 2k_a + b_{aa}[NtcA^{(a)}] - d_a[NtcA]$ and,

$\frac{d[PipX]}{dt} \leq l_x + b_{px}[2\text{-}OG] + b_{ax}[NtcA^{(a)}\text{-}PipX] - d_x[PipX]$

$\Rightarrow \frac{dW_2}{dt} \leq (l_a + l_x + 2k_a) + b_{px}[2\text{-}OG] + b_{aa}[NtcA^{(a)}] + b_{ax}[NtcA^{(a)}\text{-}PipX] - d_{w2}W_2$

where, $d_{w2} = min\{d_a, d_x\}$

$$\Rightarrow \frac{dW_2}{dt} + d_{w2} W_2 \leq \Omega_2$$

where, $\Omega_2 = (l_a + l_x + 2k_a) + b_{px}[2\text{-}OG]^* + b_{aa}[NtcA^{(a)}]^* + b_{ax}[NtcA^{(a)}\text{-}PipX]^*$ and

$[NtcA^{(a)}] \leq [NtcA^{(a)}]^*$, $[NtcA^{(a)}\text{-}PipX] \leq [NtcA^{(a)}\text{-}PipX]^*$ and $[2\text{-}OG] \leq [2\text{-}OG]^*$ for all $t \geq T^*$

Again from the theory of differential inequalities,[38] we then obtain,

$$0 < W_2([NtcA],[PipX]) < \frac{\Omega_2}{d_{w2}}(1 - e^{-d_{w2}t}) + W_2([NtcA](0),[PipX](0))e^{-d_{w2}t}$$ and for $t \to \infty$,

it follows $0 < W_2 < \frac{\Omega_2}{d_{w2}}$, hence all solution of $\left([NtcA](t),[PipX](t)\right)$ that initiate in $([NtcA](0),[PipX](0))^T \in \mathbb{R}^2$ are confined to the region: $G_2 = \{([NtcA],[PipX])^T \in \mathbb{R}^2 :$

$W_2 = \frac{\Omega_2}{d_{w2}} + \epsilon_2$ for any $\epsilon_2 > 0\}$ for all $t \geq T^{**}$, where $T^{**} > T^* > 0$ and T^{**} depends on the initial values $([NtcA](0),[PipX](0))^T \in \mathbb{R}^2$

Thus all solutions of the set of differential equations are confined in the region $G = G_1 \cup G_2 \in R^{13}$ for all $t > T^{**}$.

S4. Data fitting

In order to fit to the data,[28] the simulated concentrations of microcystin (in μM) have been converted to $\mu g\ mm^{-3}$. Molar mass of Microcystin-LR is 995.174 g (CHEBI ID: 6925)[39] which implies that 1 g of Microcystin-LR is equivalent to 0.001 mol approximately. Now, 1 μM = 10^{-6} $mol\ L^{-1}$ = 10^{-3}x 10^{-6} $g\ mm^{-3}$ = 10^{-3} $\mu g\ mm^{-3}$.

The result from the model $M(t,\hat{k})$ is fitted into the data. If ϵ be the error of the fit having independent Gaussian distribution having an unknown variance σ^2, we can write

$$y = M(t,\hat{k}) + \epsilon \quad \text{where, } \epsilon \sim N(0, I\sigma^2) \qquad \text{(S1)}$$

Here, $\hat{k} \in \mathbb{R}^n$ contains all the unknown parameters of the model and *y* contain N independent observations $y_{t_j}, j = 1, 2, ..., N$, from the data, where y_{t_j} represents the intracellular microcystin content at different time points throughout the experiment.

An independent Gaussian prior specifications for $\hat{k}$ is assumed

$$k_i \sim N(\nu_i, \eta_i^2) \text{ where, } i = 1, 2, ..n \tag{S2}$$

Gamma distribution in the following form is assumed as a prior for the inverse of error variance:

$$p(\sigma^{-2}) \sim \Gamma(\frac{n_0}{2}, \frac{n_0}{2} S_0^2), \tag{S3}$$

where n_0 and S_0^2 is interpreted as prior mean and prior accuracy of σ^2 respectively. The sum of square function, $SS(\hat{k})$ is defined as:

$$\sum_{i=1}^{N} (y_{t_i} - M(t_i; \hat{k}))^2 \tag{S4}$$

Using conditional conjugacy property of gamma distribution, the conditional distribution $p(\sigma^{-2} \mid y, \hat{k})$ is also a Gamma distribution:

$$p(\sigma^{-2} \mid y, \hat{k}) = \Gamma(\frac{n_0 + N}{2}, \frac{n_0 S_0^2 + SS(\hat{k})}{2}) \tag{S5}$$

The conditional conjugacy property makes it possible to sample and update σ^2 within each Metropolis-Hastings simulation step for the other parameters. As independent Gaussian prior distribution is assumed for $\hat{k}$, then the prior sum of squares for the given $\hat{k}$ can be calculated according to

$$SS_{pri}(\hat{k}) = \sum_{i=1}^{n} \left[\frac{k_i - \nu_i}{\eta_i} \right]^2 . \tag{S6}$$

Then assuming that σ^2 has a fixed value, the posterior distribution for $\hat{k}$ can be expressed as follows:

$$p(\hat{k} \mid y, \sigma^2) \propto exp\left\{-\frac{1}{2}\left(\frac{SS(\hat{k})}{\sigma^2} + SS_{pri}(\hat{k})\right)\right\} \quad \text{(S7)}$$

and the posterior ratio needed in the Metropolis-Hastings acceptance probability can be written as:

$$\frac{p(\hat{k}^2 \mid y, \sigma^2)}{p(\hat{k}^1 \mid y, \sigma^2)} = exp\left\{-\frac{1}{2}\left(\frac{SS(\hat{k}^2)}{\sigma^2} - \frac{SS(\hat{k}^1)}{\sigma^2}\right) + \frac{1}{2}\left(SS_{pri}(\hat{k}^2) - SS_{pri}(\hat{k}^1)\right)\right\} \quad \text{(S8)}$$

The Delayed Rejection Adaptive Metropolis algorithm (DRAM) [29, 30] was used to generate posterior distributions of the parameters with an initial burn in period of 200000 simulations. The mean of MCMC chain after 200000 iterations was calculated for each of the parameters and used as point estimates for the unknowns. The algorithm was implemented using the MCMC toolbox[31] (written by Marko Laine) in MATLAB R2012a. Geweke's Z-scores [40] were used to ensure convergence of the MCMC chains.

Table S2: Geweke Z-scores for each of the parameters

Parameters	**Geweke Z-scores**
k_m *(batch 1)*	0.99
k_m *(batch 2)*	0.97
f_{mg}	0.97
k_3	0.96
l_{mcy}	0.95
l_{gl}	0.99
d_{gl}	0.97
d_m	0.97
d	0.98

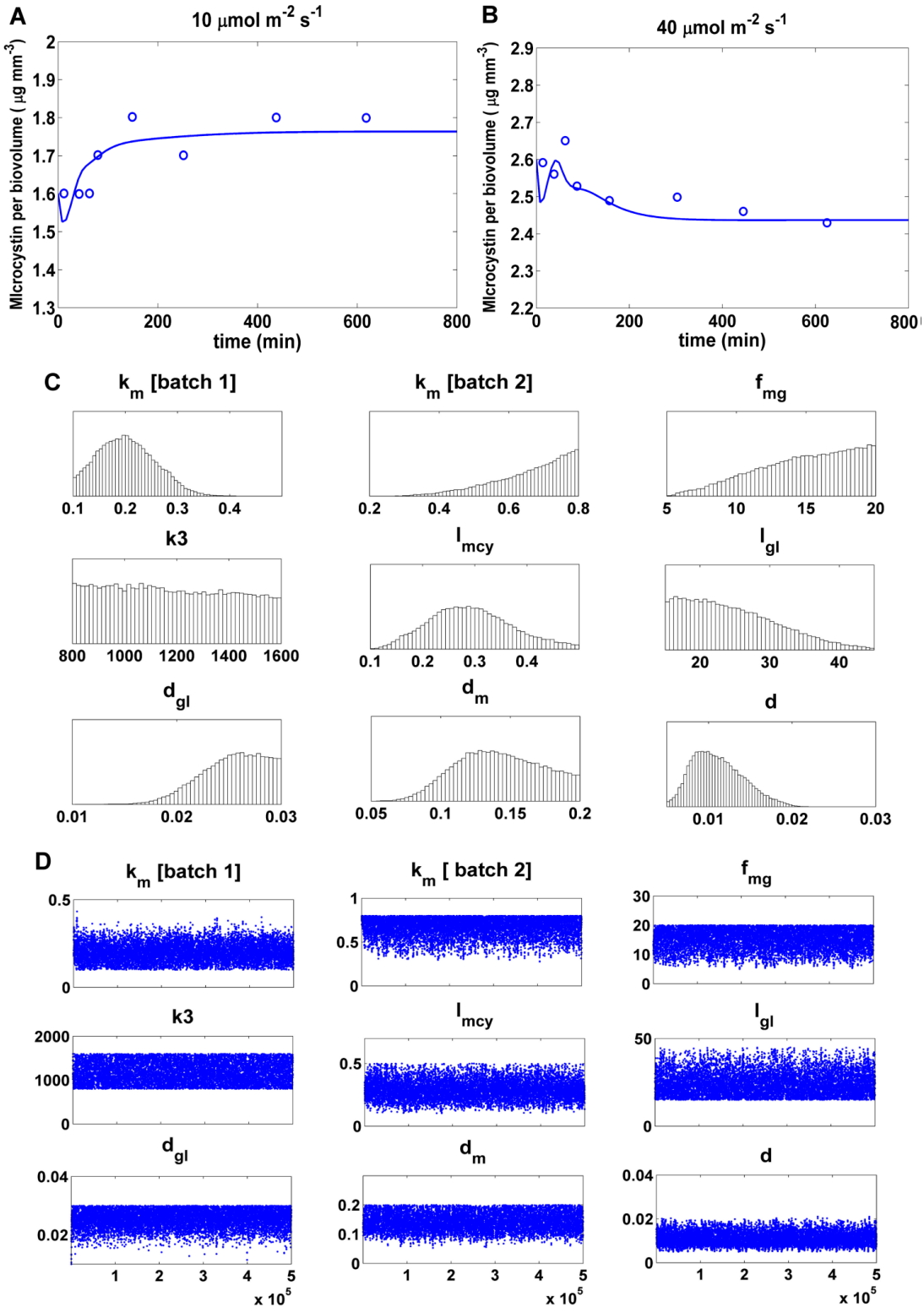

Fig S1: (A and B): Temporal plot of intracellular microcystin with the point estimate (mean of posterior distribution) for each of the parameters. Circles (o) represent real data obtained from [28]. **(C)** The marginal distributions of all estimated parameters. **(D)** Parameter trace plots of MCMC sampling demonstrating chain convergence

S5. Parameters and initial values

The parameters and initial values listed in Table S3 and S4 respectively have been used for all simulations unless mentioned otherwise:

Table S3: Parameters description and values used for simulaton

Parameters	***Description***	***Unit***	***Value***	***Literature***	***Reference***
v_{max1}	Maximal rate of GOGAT activity	$\mu M\ min^{-1}$	326	326 *U/mL* 1 *U*=1 *nM/min* is assumed	41
K_{gn}	Equilibrium dissociation constant for the dissociation of Gln from the ternary enzyme substrate complex	μM	173	0.173 *mM*	41
K_{2-og}	Equilibrium dissociation constant for the dissociation of 2-OG from the ternary enzyme substrate complex	μM	10	10 μM	41
$K_{i(gn)}$	Equilibrium dissociation constant for the dissociation of Gln from the binary enzyme substrate complex	μM	104	0.104 *mM*	41
v_{max2}	Maximal rate of GS activity	$\mu M\ min^{-1}$	150		Assumed
K_{nh}	Equilibrium dissociation constant for the dissociation of NH_4^+ from the ternary enzyme substrate complex	μM	60	0.06 *mM*	42
K_{gl}	Equilibrium dissociation constant for the dissociation of Glu from the ternary enzyme substrate complex	μM	4500	4.5 *mM*	42
$K_{i(gl)}$	Equilibrium dissociation constant for the dissociation of Glu from the binary enzyme substrate complex	μM	37200*	Calculated	42
v_{max3}	Maximal rate of GDH activity	$\mu M\ min^{-1}$	55	Alternative pathway and hence considered less than v_{max2}	Assumed
$K"_{nh}$	Equilibrium dissociation constant for the dissociation of NH_4^+ from the ternary enzyme substrate complex	μM	5800	5.8 *mM*	43

K''_{2-og}	Equilibrium dissociation constant for the dissociation of 2-OG from the ternary enzyme substrate complex	μM	260	260 μM	[43]
$K''_{i(2-og)}$	Equilibrium dissociation constant for the dissociation of 2-OG from the binary enzyme substrate complex	μM	720	720 μM	[43]
f_{ax}	Rate constant of formation of NtcA-PipX complex	$\mu M^{-1} min^{-1}$	0.1	K_d for NtcA-PipX binding 85 nM	[44]
b_{ax}	Rate constant of disscociation of NtcA-PipX complex	min^{-1}	0.0085		[44]
f_{px}	Rate constant of formation of PII-PipX complex	$\mu M^{-1} min^{-1}$	0.0001**	K_d for PII-PipX binding ~ 7 μM in the absence of 2-OG	[23, 44]
l_a	Basal production rate of NtcA	$\mu M\ min^{-1}$	0.39		Assumed[#]
d_a	Natural degradation of NtcA	min^{-1}	0.2		
l_p	Basal production rate of PII	$\mu M\ min^{-1}$	0.25		
d_p	Natural degradation of PII	min^{-1}	0.2		
l_x	Basal production rate of PipX	$\mu M\ min^{-1}$	0.08		
d_x	Natural degradation of PipX	min^{-1}	0.1		
d_{px}	Natural degradation of PII-PipX complex	min^{-1}	0.005		
f_{aa}	Rate constant of formation of NtcA-2OG complex	$\mu M^{-1} min^{-1}$	0.0001		Assumed
b_{aa}	Rate constant of dissociation of NtcA-2OG complex	min^{-1}	0.008		Assumed
d_{aa}	Natural degradation of NtcA-2OG complex	min^{-1}	0.2		Assumed[#]
l_{nh}	Rate of internal ammonium ion influx from other intracellular sources	$\mu M\ min^{-1}$	0.06		Assumed[##]
l_{og}	Rate of 2-OG influx from TCA cycle	$\mu M\ min^{-1}$	53		
d_{og}	Depletion of 2-OG due to consumption in other reactions	min^{-1}	0.12		

d_n	Natural depletion of intracellular ammonium ion or consumption into other reactions	min^{-1}	0.23		Assumed[##]
b_{px}	Rate constant of 2-OG dependent dissociation of PII-PipX	min^{-1}	0.001**	K_d for PII-PipX binding ~ 7 μM in the absence of 2-OG	23, 44
k_4	Half saturation constant of 2-OG dependent PII-PipX dissociation	μM	0.5		Assumed
k_a	Maximal rate of synthesis of NtcA	$\mu M\ min^{-1}$	0.17		Assumed
θ_1	Half saturation constant for synthesis of NtcA due to NtcA$^{(a)}$	μM^2	0.42	Assumed to be less than θ_3	Assumed
θ_2	Half saturation constant for synthesis of NtcA due to NtcA$^{(a)}$-PipX	μM^2	0.11	Assumed to be less than θ_1	Assumed
c_{ax}	rate constant of nitrogen uptake under the influence of NtcA$^{(a)}$ and NtcA$^{(a)}$-PipX	min^{-1}	12.57		Assumed
k_1	Half saturation constant of nitrogen uptake due to NtcA$^{(a)}$	μM	30	k_1 assumed greater than k_2	Assumed
k_2	Half saturation constant of nitrogen uptake due to NtcA$^{(a)}$-PipX	μM	7	k_m for uptake of ammonium= 7 µM	27
k_m	Maximal rate of synthesis of Mcy protein	$\mu M\ min^{-1}$	0.2030 (batch 1) 0.6632 (batch 2)		Estimated
θ_3	Half saturation constant for synthesis of Mcy due to NtcA$^{(a)}$	μM^3	0.625***	K_d for NtcA-mcy (in presence of 2-OG) =0.625 μM	14
θ_4	Half saturation constant for synthesis of Mcy due to NtcA$^{(a)}$-PipX	μM^3	0.325	Assumed to be less than θ_3	Assumed
d_m	Natural degradation of Mcy protein	min^{-1}	0.1425		Estimated
f_{mg}	Rate constant of intracellular microcystin production	min^{-1}	14.8675		Estimated
k_3	Half saturation constant of intracellular microcystin production	μM	1183.7		Estimated

d	depletion of intracellular microcystin due natural degradation or transport to extracellular environment	min^{-1}	0.0111		Estimated
l_{mcy}	Basal production rate of Mcy	$\mu M\ min^{-1}$	0.2931		Estimated
L	Rate of formation of external nitrogen in the growing medium	$\mu M\ min^{-1}$	250		Assumed###
d_N	natural depletion of the external nitrogen	min^{-1}	0.9		Assumed###
d_{ax}	Natural degradation of NtcA-PipX complex	min^{-1}	0.01		Assumed#
l_{gl}	Rate of glutamate influx from other intracellular sources	$\mu M\ min^{-1}$	24.6664		Estimated
l_{gn}	Rate of glutamine influx from other intracellular sources	$\mu M\ min^{-1}$	16		Assumed####
d_{gl}	depletion of glutamate into other reactions	min^{-1}	0.0253		Estimated
d_{gn}	depletion of glutamine into other reactions	min^{-1}	0.08		Assumed####

Dry mass of *Microcystis aeruginosa* was reported to be 438.4 *fg* μm^{-3} [32] and the protein content was assumed to be 30% of the dry biomass [33] which is approximately 130 *fg* μm^{-3} (130 x 10^3 *mg/L*). Hence, it can be assumed that 1 mg of protein to be equivalent to 1/(130 x 10^3) L of volume within a cyanobacterium cell. Hence 1 nmoles/mg of protein ~ 130 x 10^3 nmoles/L = 130 x 10^3 nM =130 µM.

* For fixed glutamate concentration approximately 3 mM, a value of $K_{NH_4^+}$ =0.3216 mM very close to the average of the two fitted value of $K_{NH_4^+}$ is assumed, and $K_{i(gl)}$ is calculated using the formula $K_{NH_4^+} = \frac{K_{nh}(K_{i(gl)} + [Glu])}{K_{gl} + [Glu]}$ [45]

** As 2-oxoglutarate assists in PipX dissociation from PII, the K_d value in presence of 2-OG, is assumed to be 10 μM . Further, it was assumed, b_{px} / f_{px} =10 μM.

*** θ_3 is assumed equal to K_d for NtcA-mcy binding.

The intracellular concentration of signalling proteins/transcription factors can range between 10 nM – 1 µM.[46] The formation and degradation rates of the proteins and complexes have been assumed so that the intracellular concentration is always of the order of 1 µM.

The k_m for glutamine synthetase ranges from 20-170 µM for ammonium[17] and intracellular 2-oxoglutarate concentration ranges from 60-440 µM.[16] The formation and depletion rate of 2-OG and ammonium in our

model were so assumed that simulations yielded an intracellular concentration of around 50 µM and 300 µM for nitrogen and 2-oxoglutarate respectively.

Surface water may contain ammonium upto 12 mg/litre.[47] Molar mass of ammonium is 18g (CHEBI)[39]. Hence, 1g can be written as 1/18 mol = 1/18 x 10^6 µmol. Thus 12 mg/litre = 12 x 10^{-3} g/litre = 0.66667 x 10^3 µmol/litre = 666.67 µM. Our simulation results only reach a value of 250 µM for excess ammonium condition which is well within the reported value. Also, we used L=1µM to produce nitrogen starved condition and the aim was to observe the system behaviour under very almost no available nitrogen.

Muro-Pastor et al.[15] in their study have measured the intracellular concentration of glutamine in cyanobacteria to be 0-85 nmoles/mg protein. This can be scaled using dry mass of *Microcystis aeruginosa* and the protein content (detailed description shown below) to be approximately 0-11050 µM. In our simulation, the glutamine formation rate and depletion rate have been assumed such that all our simulations lead to intracellular glutamine concentration which is well within the reported range.

Table S4: Symbols representing all state variables and their initial values used for simulations

Variables	***Symbols***	***Initial values***	***Reference***
External ammonium ion	$[NH_4^+{}_{(ext)}]$	10000	assumed
Glutamate	[Glu]	600	[15]
Glutamine	[Gln]	11000	[15]
2-oxoglutarate	[2-OG]	10	assumed
Internal ammonium ion	$[NH_4^+]$	200	assumed
NtcA	[NtcA]	0.2	assumed
PII	[PII]	2	assumed
PipX	[PipX]	0.25	assumed
NtcA-2-OG complex	$[NtcA^{(a)}]$	0.05	assumed
NtcA-2-OG-PipX complex	$[NtcA^{(a)}$-PipX]	1	assumed
PII-PipX complex	[PII-PipX]	1	assumed
Mcy enzyme	[Mcy]	0.1	assumed
Microcystin	[MC]	1600 (batch 1) 2600 (batch 2)	[28]

*All the initial values are taken in μM

S6. Equilibrium points and Stability analysis

The interior equilibrium point $X^* \in \mathbb{R}_+^{13}$ for the system can be calculated by using the following set of algebraic equations:

$$L - c_{ax}\left(\frac{[NtcA^{(a)}]}{k_1 + [NH_{4(ext)}^+]} + \frac{[NtcA^{(a)}\text{-}PipX]}{k_2 + [NH_{4(ext)}^+]}\right)[NH_{4(ext)}^+] - d_N[NH_{4(ext)}^+] = 0$$

$$l_{gl} + V_{GOGAT} - V_{GS} + V_{GDH} - f_{mg}\frac{[Mcy][Glu]}{k_3 + [Glu]} - d_{gl}[Glu] = 0$$

$$l_{gn} + V_{GS} - V_{GOGAT} - d_{gn}[Gln] = 0$$

$$l_{og} - V_{GOGAT} - V_{GDH} - f_{aa}[NtcA][2\text{-}OG] + b_{aa}[NtcA^{(a)}] - d_{og}[2\text{-}OG] = 0$$

$$l_{nh} - V_{GS} - V_{GDH} + c_{ax}\left(\frac{[NtcA^{(a)}]}{k_1 + [NH_{4(ext)}^+]} + \frac{[NtcA^{(a)}\text{-}PipX]}{k_2 + [NH_{4(ext)}^+]}\right)[NH_{4(ext)}^+] - d_n[NH_4^+] = 0$$

$$l_a + k_a\left(\frac{[NtcA^{(a)}]^2}{\theta_1 + [NtcA^{(a)}]^2} + \frac{[NtcA^{(a)}\text{-}PipX]^2}{\theta_2 + [NtcA^{(a)}\text{-}PipX]^2}\right) - f_{aa}[NtcA][2\text{-}OG] + b_{aa}[NtcA^{(a)}] - d_a[NtcA] = 0$$

$$f_{aa}[NtcA][2\text{-}OG] - b_{aa}[NtcA^{(a)}] - f_{ax}[NtcA^{(a)}][PipX] + b_{ax}[NtcA^{(a)}\text{-}PipX] - d_{aa}[NtcA^{(a)}] = 0$$

$$l_p - f_{px}[PII][PipX] + \frac{b_{px}[2\text{-}OG][PII\text{-}PipX]}{k_4 + [PII\text{-}PipX]} - d_p[PII] = 0$$

$$l_x - f_{px}[PII][PipX] - f_{ax}[NtcA^{(a)}][PipX] + \frac{b_{px}[2\text{-}OG][PII\text{-}PipX]}{k_4 + [PII\text{-}PipX]} + b_{ax}[NtcA^{(a)}\text{-}PipX] - d_x[PipX] = 0$$

$$f_{ax}[NtcA^{(a)}][PipX] - (b_{ax} + d_{ax})[NtcA^{(a)}\text{-}PipX] = 0$$

$$f_{px}[PII][PipX] - \frac{b_{px}[2\text{-}OG][PII\text{-}PipX]}{k_4 + [PII\text{-}PipX]} - d_{px}[PII\text{-}PipX] = 0$$

$$l_{mcy} + k_m\left(\frac{[NtcA^{(a)}]^3}{\theta_3 + [NtcA^{(a)}]^3} + \frac{[NtcA^{(a)}\text{-}PipX]^3}{\theta_4 + [NtcA^{(a)}\text{-}PipX]^3}\right) - d_m[Mcy] = 0$$

$$f_{mg}\frac{[Mcy][Glu]}{k_3 + [Glu]} - d[MC] = 0 \qquad \text{(S9.1-S9.13)}$$

To investigate whether the toxin free equilibrium can exist for our system:

Let [MC] =0,

Then from (S9.13), $f_{mg}\frac{[Mcy][Glu]}{k_3 + [Glu]} = 0$.

$\Rightarrow$ either, $[Glu] = 0$ or, $[Mcy]=0$

Hence, from equation (S9.2) and (S9.12),

$$l_{gl} + V_{GOGAT} + V_{GDH} = 0 \qquad \text{(S10.1)}$$

or , $$l_{mcy} + k_m\left(\frac{[NtcA^{(a)}]^3}{\theta_3 + [NtcA^{(a)}]^3} + \frac{[NtcA^{(a)}\text{-}PipX]^3}{\theta_4 + [NtcA^{(a)}\text{-}PipX]^3}\right) = 0 \qquad \text{(S10.2)}$$

Both the equations S10.1 and S10.2 cannot be true for non-zero positive parameter values. Hence, it is obvious that the toxin free equilibrium cannot exist which ensures that there can be no set of parameter within our considered ranges which leads to complete abolishment of intracellular microcystin levels.

To ensure positivity and existence of the interior equilibrium solutions, Latin Hypercube Sampling (LHS) was used to generate 100000 random parameter sets within the defined ranges (Table S5) and the model simulations of the range of 10^6 min were performed for each such combination. It was observed that each model simulation led to positive interior equilibrium solution.

Further to check the stability of the system, the Jacobian matrix J was calculated using Symbolic Math Toolbox in MATLAB 2012a. The sensitive parameters and other parameters considered in the result section were largely varied, and the steady state solutions $X^* \in \mathbb{R}_+^{13}$ for each set of parameters were obtained from simulations. $J^*=J|_{X^*}$ was obtained at each of these steady states and the eigen values were calculated numerically. It was observed that the real part of all the eigen

values were negative thus confirming a stable steady state of the positive interior equilibrium point. Stability regions are shown in Fig S2 for few parametric combinations.

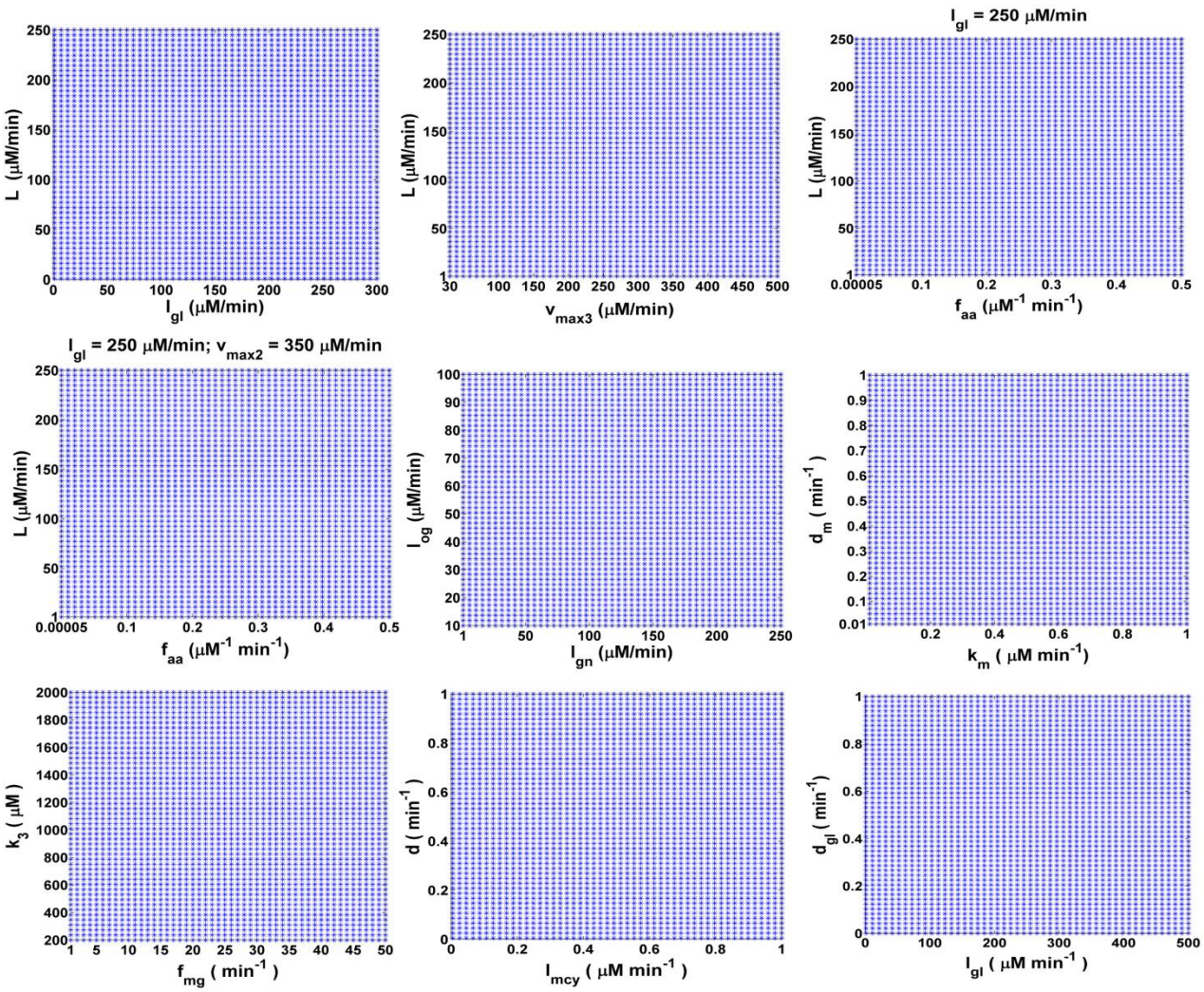

Fig S2: Regions of stability for different parametric combinations

S7. Global Sensitivity Analysis

Extend Fourier Amplitude Sensitivity Test (eFAST) was used to carry out a parameter sensitivity analysis. The algorithm assigns each input parameter a sinusoidal function of a particular frequency that determines the parameter value on the basis of sample number from 1 through N_S, the total number of samples per search curve. The choice of the sinusoidal function depends on the type of distribution specified for each parameter. In order to avoid same samples being drawn, the algorithm is repeated N_R times, by introducing random phase shift of the sinusoidal function at each iteration.[48]

For each of the i^{th} parameter, we calculate two sensitivity indices, *viz.*, the first order sensitivity index, S_i and the total order sensitivity index, S_{Ti}. S_i denotes the fraction of model output variance which can be explained by input variation of a parameter. In order to calculate S_{Ti}, the summed sensitivity index of all the parameters except i, is calculated using their corresponding frequency. Then, S_{Ti} is calculated as the remaining variance after the contribution of the complementary set S_{ci} is removed.

$S_{Ti}=1-S_{ci}$

Parameter sensitivity analysis was carried out using the whole set of parameters [k=52] and a dummy parameter, taking microcystin [MC] concentration at 200 and 10000 minutes, as the response variable. 513 samples were chosen per search curve and resampling of the frequency search curves was carried out 5 times [N_S=513, N_R=5]. Hence, the result is an outcome of total N= $53\times513\times5=135945$ model evaluations. A t-test is carried out on data generated by resampling in order to compare the distributions of S_i^j or S_{Ti}^j [j=1,2,..,N_R] with S_{dummy}^j or S_{Tdummy}^j.[48]

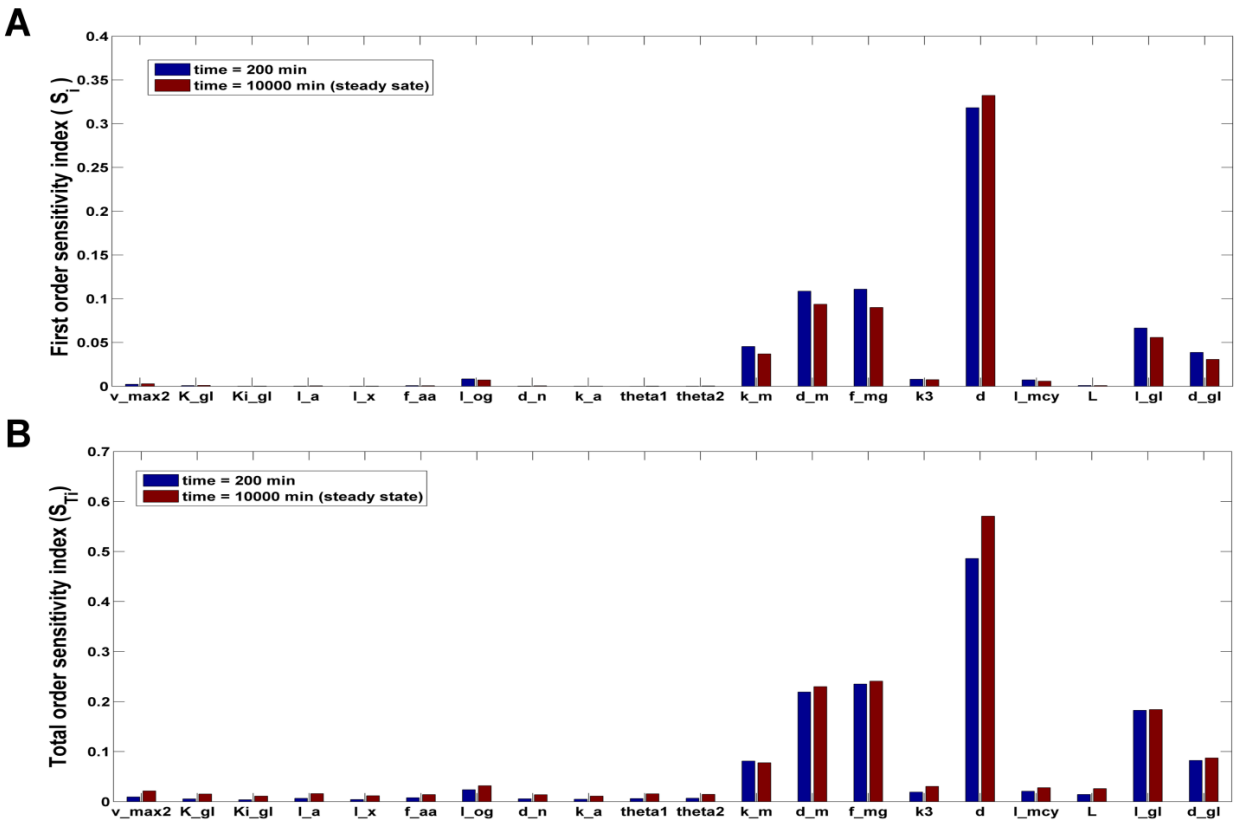

Fig. S3: First order and total order sensitivity index for significant parameters ($p<0.05$)

Table S5: The sensitivity indices for different parameters with respect to microcystin concentration at 200 min and 10000 min (* p-value < 0.01; **p-value < 0.05)

Parameters	***Range***	***S_i (200 min)***	***S_i (10000 min)***	***S_{Ti} (200 min)***	***S_{Ti} (10000 min)***
v_{max1}	[60 600]	0.0001	0.0002	0.0043	0.0121
K_{gn}	[30 300]	0.0001	0.0002	0.0037	0.0112
K_{2-og}	[5 50]	0.0001	0.0002	0.0027	0.0103
$K_{i(gn)}$	[20 200]	0.0001	0.0002	0.0041	0.0127
v_{max2}	[60 600]	0.0023**	0.0029**	0.0093	0.0214**
K_{nh}	[10 100]	0.0003	0.0004	0.0050	0.0144
K_{gl}	[600 6000]	0.0008**	0.0010	0.0055	0.0151
$K_{i(gl)}$	[4000 40000]	0.0002**	0.0003	0.0037	0.0111
v_{max3}	[30 500]	0.0000	0.0002	0.0028	0.0111
$K"_{nh}$	[700 7000]	0.0001	0.0003	0.0035	0.0119
$K"_{2-og}$	[40 400]	0.0001	0.0002	0.0050	0.0130
$K"_{i(2-og)}$	[100 1000]	0.0001	0.0003	0.0062	0.0154
f_{ax}	[0.02 0.2]	0.0001	0.0002	0.0036	0.0121
b_{ax}	[0.001 0.01]	0.0001	0.0002	0.0064	0.0162
f_{px}	[0.00005 0.5]	0.0001	0.0002	0.0047	0.0135
l_a	[0.06 0.6]	0.0003**	0.0005	0.0066**	0.0160
d_a	[0.03 0.3]	0.0000	0.0001	0.0029	0.0088
l_p	[0.1 0.7]	0.0001	0.0003	0.0066	0.0146
d_p	[0.03 0.3]	0.0001	0.0003	0.0055	0.0144
l_x	[0.07 0.7]	0.0002**	0.0003	0.0043	0.0118
d_x	[0.015 0.15]	0.0001	0.0003	0.0036	0.0116
d_{px}	[0.001 0.01]	0.0001	0.0002	0.0042	0.0126
f_{aa}	[0.00005 0.5]	0.0008**	0.0007	0.0078	0.0141
b_{aa}	[0.001 0.01]	0.0001	0.0003	0.0040	0.0127
d_{aa}	[0.03 0.3]	0.0003	0.0006	0.0071	0.0152
l_{nh}	[0.05 0.5]	0.0000	0.0001	0.0032	0.0113
l_{og}	[10 100]	0.0084*	0.0072*	0.0238**	0.0318**
d_{og}	[0.03 0.3]	0.0001	0.0003	0.0045	0.0119
d_n	[0.03 0.3]	0.0003**	0.0006	0.0056**	0.0140
b_{px}	[0.0005 0.05]	0.0000	0.0002	0.0030	0.0110
k_4	[0.09 0.9]	0.0001	0.0002	0.0042	0.0127

k_a	[0.05 0.5]	0.0002**	0.0002	0.0048	0.0110
θ_1	[0.06 0.6]	0.0001	0.0003	0.0062**	0.0156
θ_2	[0.06 0.6]	0.0002	0.0004	0.0068**	0.0144
c_{ax}	[5 50]	0.0002	0.0003	0.0050	0.0116
k_1	[4 40]	0.0001	0.0003	0.0051	0.0159
k_2	[4 40]	0.0000	0.0002	0.0032	0.0115
k_m	[0.09 0.9]	0.0455*	0.0370*	0.0811*	0.0777**
θ_3	[0.08 0.8]	0.0001	0.0002	0.0036	0.0115
θ_4	[0.08 0.8]	0.0000	0.0002	0.0036	0.0108
d_m	[0.02 0.2]	0.1087*	0.0938*	0.2192*	0.2299*
f_{mg}	[1 20]	0.1109*	0.0900*	0.2350*	0.2409*
k_3	[800 1600]	0.0081*	0.0076*	0.0191*	0.0306*
d	[0.005 0.05]	0.3182*	0.3323*	0.4861*	0.5706*
l_{mcy}	[0.06 0.6]	0.0073**	0.0058**	0.0207*	0.0279**
L	[1 500]	0.0009**	0.0009**	0.0144	0.0259
d_N	[0.09 0.9]	0.0001	0.0002	0.0032	0.0103
d_{ax}	[0.002 0.02]	0.0001	0.0003	0.0059	0.0138
l_{gl}	[1 300]	0.0665*	0.0558*	0.1825*	0.1840*
l_{gn}	[1 250]	0.0002	0.0003	0.0048	0.0125
d_{gl}	[0.003 0.3]	0.0387*	0.0307*	0.0824*	0.0873*
d_{gn}	[0.02 0.2]	0.0000	0.0002	0.0028	0.0113
dummy	[1 10]	0.0001	0.0003	0.0043	0.0134

S8. Change in microcystin under varying nitrogen and glutamate conditions

When glutamate influx into the system is low [l_{gl} =24.6664 $\mu M\ min^{-1}$ (default estimated value)], difference between microcystin under nitrogen limitation and nitrogen sufficient conditions remain low due to limitation of substrate, thereby eliminating the effect of environmental nitrogen (Fig S4 H). Low glutamate influx leads to reduced activity of GS-GOGAT thereby increasing 2-OG levels (Fig S4 E) leading to an amplified Mcy steady state value (through NtcA-2OG) of around 6μM (Fig S4 G). Even, nitrogen limitation under this condition was unable to increase 2-OG sufficiently leading to negligible increase in Mcy concentration up to (6.193 μM) (Fig S4 G). But, when glutamate influx into the system is high (l_{gl} =250 $\mu M\ min^{-1}$), although intracellular microcystin concentration increases (6386 μM) due to increase in the substrate concentration (Fig S4 H), a higher influx into the GS-GOGAT (evident from increased glutamine concentration), leads to a greater consumption of 2-OG thus lowering Mcy levels (5.5 μM) (Fig S4 E, G). Further, creating a

nitrogen deficient scenario under such condition, led to a further increase in Mcy concentration 6.17 μM (Fig S4 G). The increased enzyme level combined with higher substrate glutamate leads to even higher microcystin concentrations (7092 μM) (Fig S4 H).

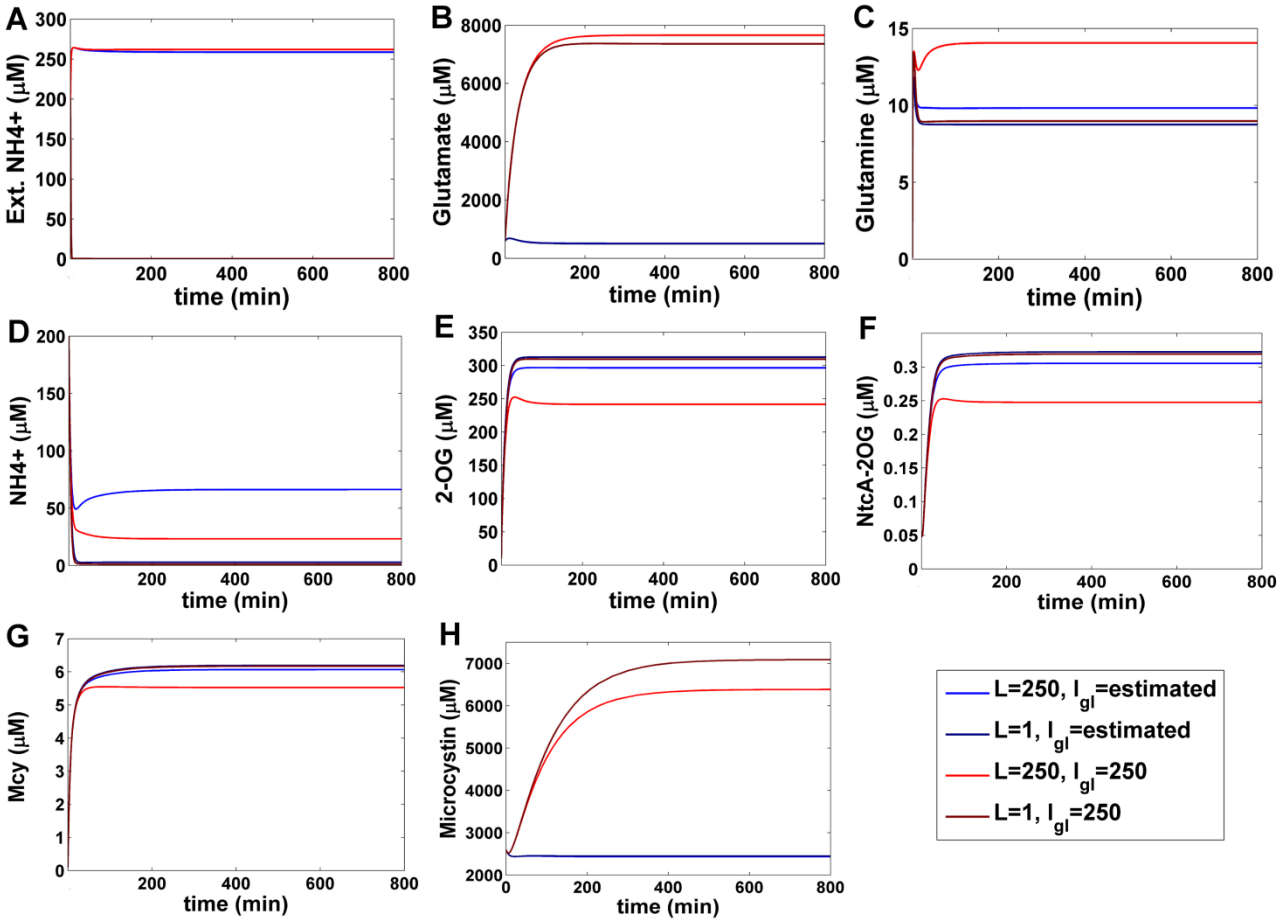

Fig S4: Temporal behaviour of different state variables considered in our models for different nitrogen (L) and glutamate influx (l_{gl}) scenario. (In order to observe the changes in external nitrogen and glutamine, their initial values are considered to be 200 µM and 0.1 µM respectively.)

S8.1 *Reversal of microcystin-nitrogen relationship*

A reversal of microcystin behaviour under nitrogen limitation was noted at increased v_{max3} when simulations were carried out at low glutamate conditions. Under nitrogen deficient conditions increasing v_{max3} had no effect on microcystin production (Fig S5 I). But, under sufficient nitrogen availability, when the activity of GDH is dominating (v_{max3}=500 $\mu M\ min^{-1}$), the glutamate produced is directly diverted to microcystin production rather than GS-GOGAT (Fig S9 B), which is evident from the glutamine temporal plot where no change in behaviour of glutamine is observed for

different v_{max3} (Fig S9 C). This increases the microcystin concentration leading to a relative increase of microcystin level under nitrogen excess conditions (Fig S9 I).

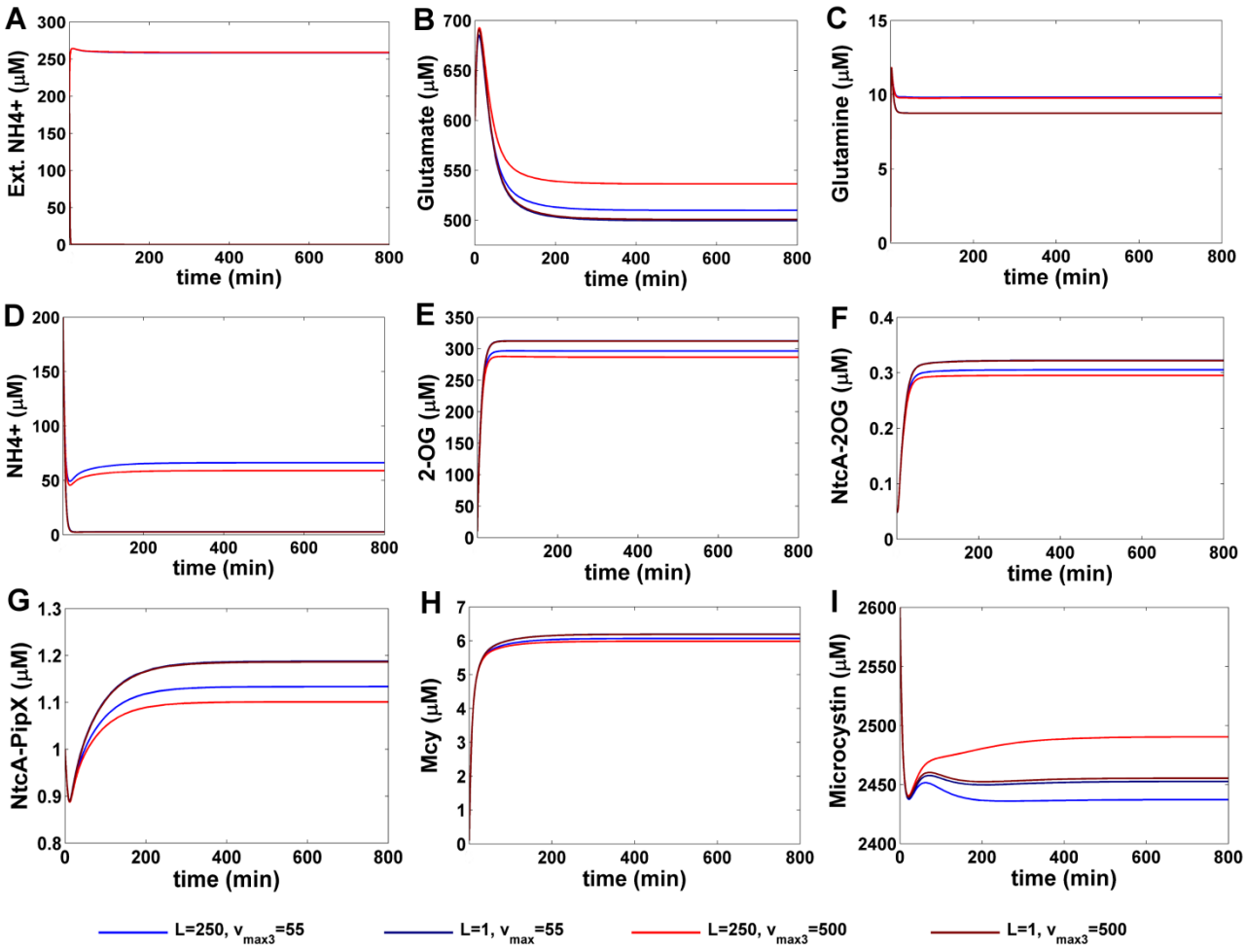

Fig S5: Temporal behaviour of different state variables for different GDH activity (v_{max3}) and nitrogen condition (L) (In order to observe the changes in external nitrogen and glutamine, their initial values are considered to be 200 μM and 0.1 μM respectively.)

S9. Opposite behaviour of glutamate steady state under nitrogen deficiency

Under high influx of glutamate to the system (l_{gl}=250 $\mu M\ min^{-1}$) when the NtcA-2OG formation rate is higher (f_{aa}=0.1 $\mu M^{-1} min^{-1}$), i.e., 2-OG is preferred in the gene regulation of Mcy via NtcA-2OG complex formation rather than the GS-GOGAT (Fig S6 F and G), glutamate concentration could only accumulate upto the concentration of around 5000 μM (Fig S6 B). This is because of the inoperable GOGAT due to 2-OG unavailability (Fig S6 E) and excess formation of Mcy which was able to divert all the glutamate into microcystin production (Fig S6 I). Hence under such condition, GS solely acts as a glutamate sink as is evident from the increased glutamine concentration (Fig S6 C). Introducing nitrogen starvation in this condition causes GS to stop, accumulating relatively higher glutamate concentration (Fig S6 B).

In order to support this observation, v_{max2} was increased to 350 $\mu M\ min^{-1}$. This increases glutamate leakage into GS under nitrogen sufficient condition (evident from higher level of glutamine concentration) (Fig S6 C) thus decreasing glutamate as well as microcystin levels (Fig S6 B, I). A nitrogen starvation scenario under such conditions stops this increased leakage of glutamate thus bringing about a relatively higher change in glutamate as well as microcystin concentration (See main article Fig. 4D and Fig S6 B, I). Also, increased v_{max2} under nitrogen sufficient levels ensures that the GS-GOGAT runs with a lower strength thereby leading to an extra accumulation of glutamate. Consequently, the relative difference in glutamate under the two nitrogen condition is lesser as compared to that of microcystin (See main article Fig. 4E).

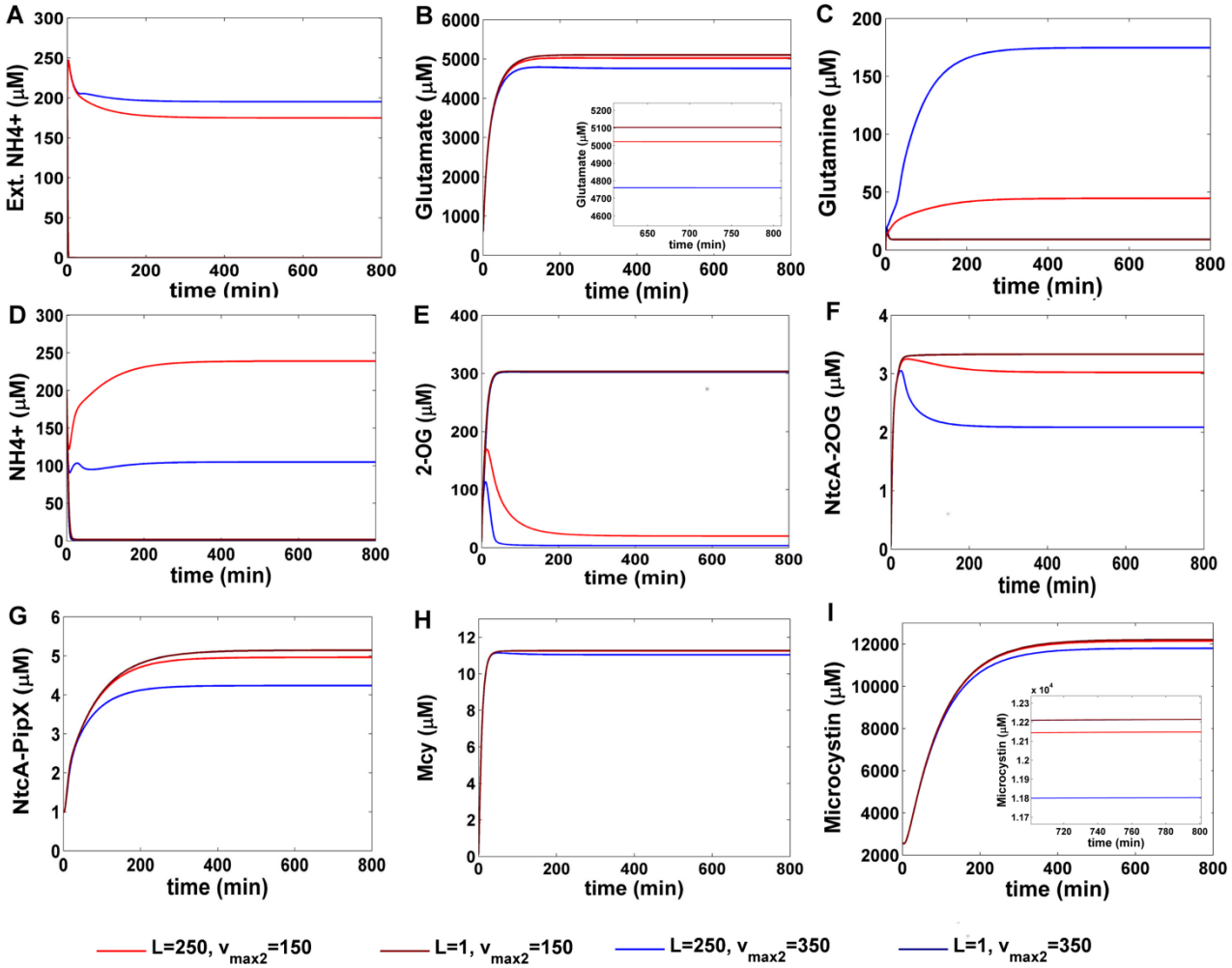

Fig S6: Temporal plots of different state variables for different GS activity (v_{max2}) and nitrogen conditions (L) when f_{aa} = 0.1 $\mu M^{-1}min^{-1}$ *and* l_{gl}=*250* $\mu M\ min^{-1}$. (In order to observe the changes in external nitrogen and glutamine, their initial values are considered to be 200 µM and 0.1 µM respectively.)

S10. Behaviour of microcystin affected by indirect regulators

S10.1 *Effect of glutamine influx on steady state microcystin levels*

As the rate of glutamine influx into the system increases, subsequently the steady state levels of glutamate increased due to increased activity of the GOGAT. This leads to decreased concentration of the 2-OG (Fig S7 D) leading to subsequent decrease in Mcy concentration (Fig S7 H). For l_{gn}=10 $\mu M\ min^{-1}$ and 28 $\mu M\ min^{-1}$, glutamate increases initially due to GOGAT activity, but there is a subsequent decrease in concentration signifying microcystin formation under enough availability of Mcy enzyme (Fig S7 A). For l_{gn}=45 $\mu M\ min^{-1}$, the transient behaviour of glutamate also changes along with steady state levels (Fig S7 A).

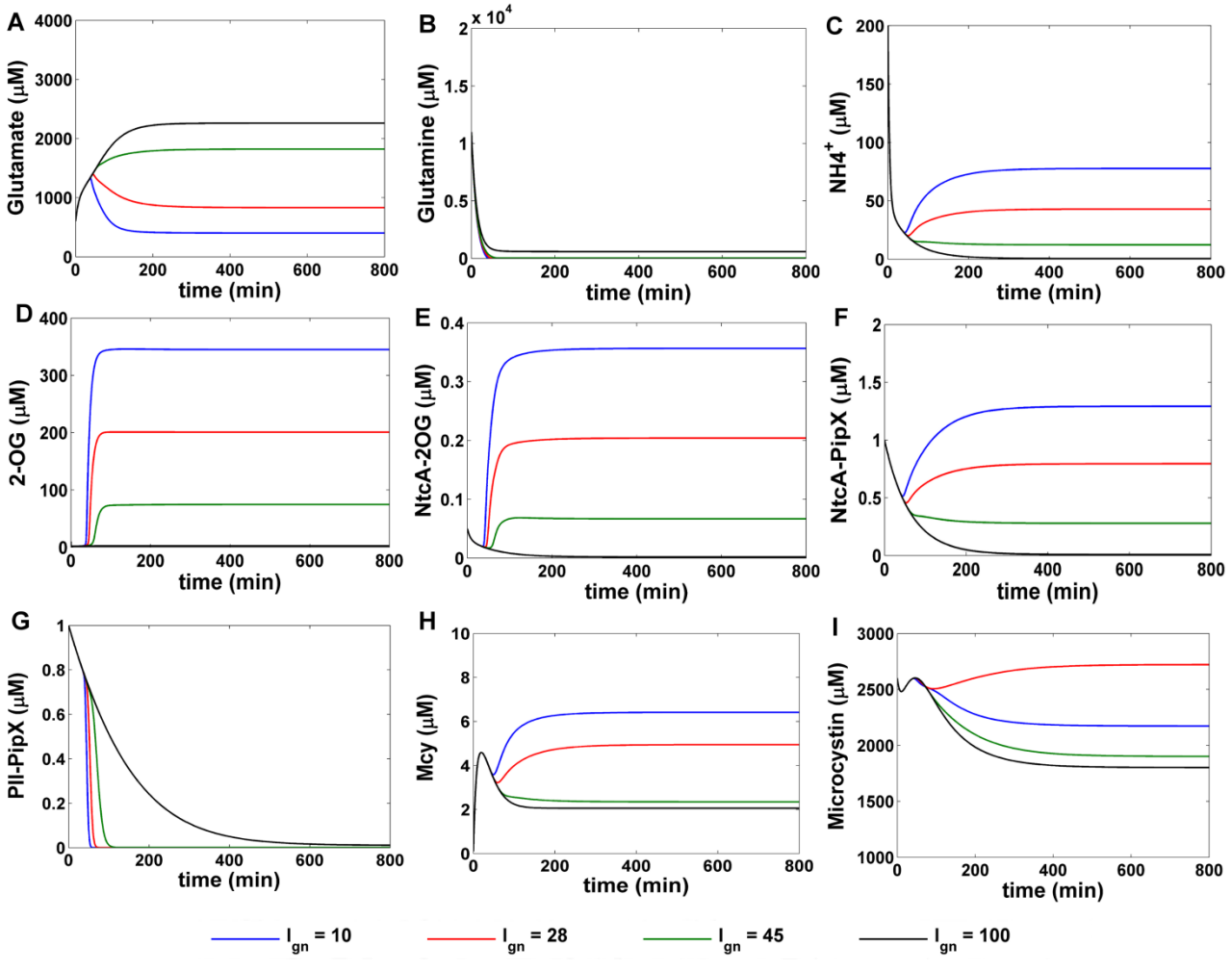

Fig S7: Temporal behaviour of different components for different glutamine influx (l_{gn}=10, 28, 45, 100 $\mu M\ min^{-1}$) for l_{og}=53 $\mu M\ min^{-1}$

Although, initially the glutamate is consumed into microcystin (up to around 40 *min* - 45 *min*), further in time, glutamate accumulation increases as the flux of glutamine into GOGAT is very high affecting 2-OG dependent Mcy enzyme levels (Fig S7 D, H). Microcystin reaches very low levels as the available Mcy enzyme in comparison to substrate glutamate is sufficiently low (Fig S7 I). A further increase in glutamine influx rates l_{gn} =100 $\mu M\ min^{-1}$ represents the increased glutamine influx scenario where whole 2-OG was consumed in GS-GOGAT (Fig S7 D) thereby producing lowest saturating microcystin levels (Fig S7 I).

S10.2 *Transient effect of glutamine on microcystin synthetase transcription*

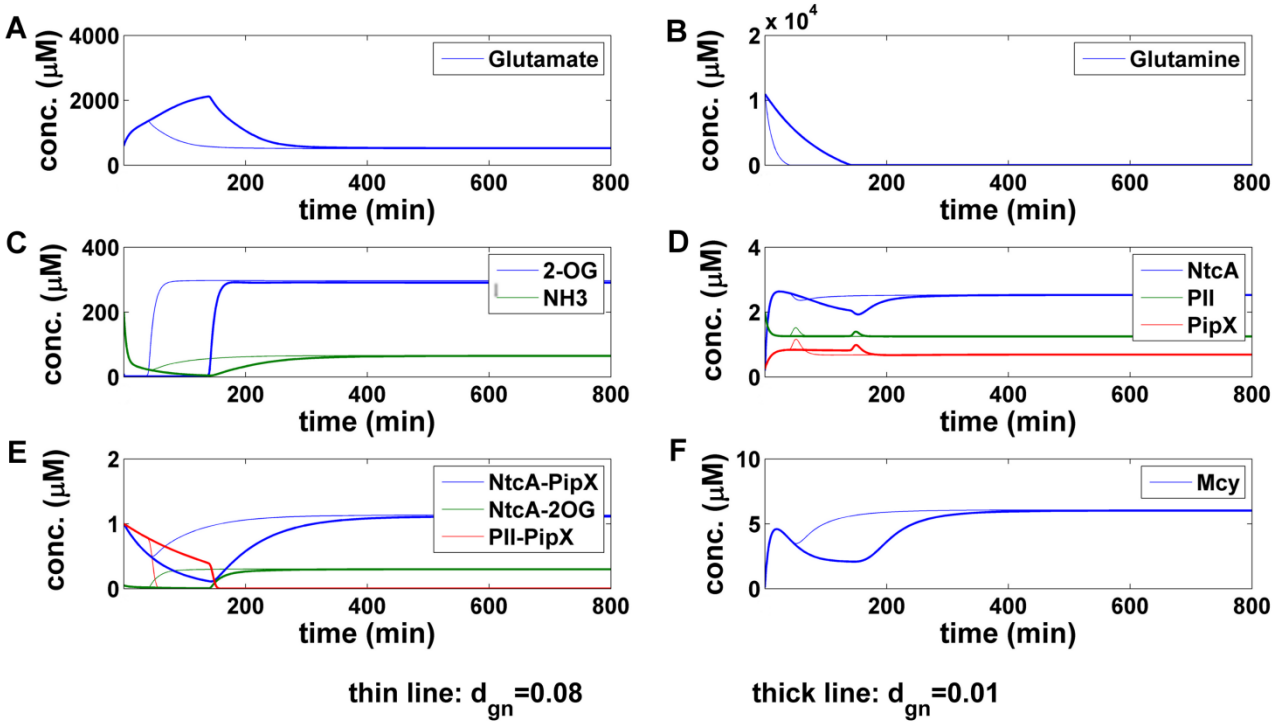

Fig. S8: Delayed production of Mcy with decreasing d_{gn}. The thick lines represent d_{gn}=0.01 min^{-1} and thin lines represent d_{gn}=0.08 min^{-1}.

Initially the 2-OG available is preferred towards the GS-GOGAT rather than the gene regulatory network of microcystin. The operation of GOGAT increases glutamate until 40 *min* (at d_{gn}=0.08 min^{-1}) by which time glutamine concentration reaches very low value (Fig S8 A, B). This signifies that the inflow and outflow of metabolites through GS-GOGAT cycle is nearly balanced thereby making the 2-OG available for Mcy regulation (2-OG switch to higher concentration) (Fig S8 C). With increasing 2-OG concentration, the NtcA-2OG concentration increases which subsequently leads to increase in NtcA-2OG-PipX and Mcy transcription (Fig S8 E, F). In order to study the effect of glutamine, the rate of depletion of glutamine was decreased (d_{gn}=0.01 min^{-1}) leading to prolonged high activity of the GS which simultaneously enters into the GOGAT to synthesize

sufficient glutamate (Fig S8 A). This can be confirmed as the glutamine reaches the steady state slower in this case and the glutamate increases initially upto 140 *min* after which it is consumed into microcystin (Fig S8 A and B). Although the same steady state level was maintained, there is a corresponding time delay in the 2-OG switch which delayed production of NtcA-2OG and subsequently Mcy (Fig S8 C, F).

S10.3 *Effect of the signalling protein PII on microcystin levels*

Changes in the PII protein considered in our model did not show significant change in microcystin levels. When simulated without PII protein there were only transient changes in the PipX concentration due to removal of binding constraint provided by PII (Fig S9 A, B). Subsequent increase in the affinity of PipX for PII (f_{px} = 0.0001 $\mu M^{-1}min^{-1}$ and f_{px} = 0.1 $\mu M^{-1}min^{-1}$) demonstrated no distinct effect on the microcystin steady state level (Fig S9 F). But at very high sequestration of PipX by PII (f_{px} = 0.5 $\mu M^{-1}min^{-1}$) the free PipX concentration decreases (Fig S9 B) thus decreasing the NtcA-PipX concentration (Fig S9 D). These in turn led to a decreased Mcy and hence relatively lower microcystin levels, although the relative difference in steady state microcystin remains still low (Fig S9 E, F).

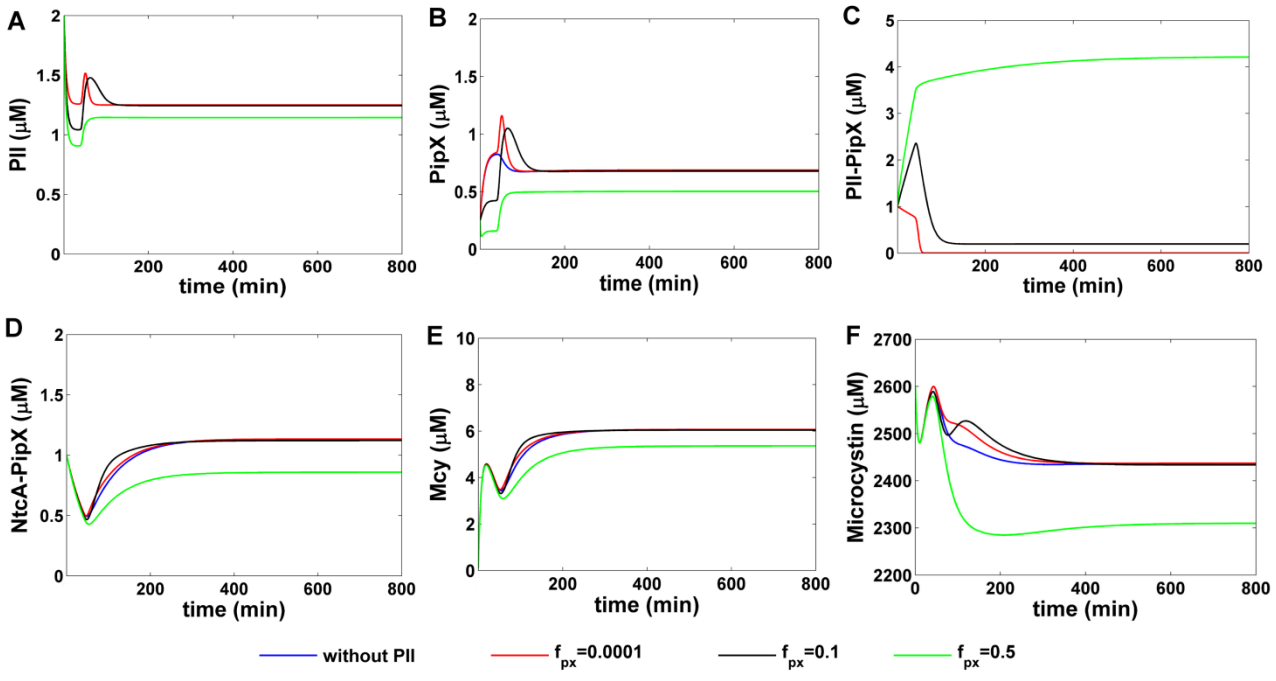

Fig S9: Time plots of different state variables without PII, and with PII for different f_{px}

References cited in this Supplementary Text are provided in the Reference list of the Main Article